STRUCTURAL SCIENCE
CRYSTAL ENGINEERING
MATERIALS

Volume 75 (2019)

Supporting information for article:

Developing new SrI2 and β-d-fructopyranose-based metal–organic frameworks with NLO properties

Domenica Marabello, Paola Antoniotti, Paola Benzi, Elena Cariati, Leonardo Lo Presti and Carlo Canepa

Section S1. Crystallographic results

Table S1. Details on crystal data and data collections and refinements.

	Compound **1**	Compound **2**	Compound **3**
Formula	$[Sr(fructose)_2]I_2$	$[Sr_2(fructose)_3]I_4 \cdot H_2O$	$[Sr(fructose)(H_2O)_3I]I$
Empirical formula	$C_{12}H_{24}O_{12}SrI_2$	$C_{18}H_{41}O_{21}Sr_2I_4$	$C_6H_{18}O_9SrI_2$
Formula weight	701.73	1276.35	575.62
Temperature/K	293(2)	293(2)	293(2)
Crystal system	monoclinic	orthorhombic	orthorhombic
Space group	$P2_1$	$P2_12_12_1$	$P2_12_12_1$
a/Å	7.8592(4)	12.3717(2)	9.1192(3)
b/Å	12.9355(5)	17.4352(3)	13.0908(5)
c/Å	9.9504(3)	17.6607(3)	13.5504(8)
α/°	90	90	90
β/°	92.803(4)	90	90
γ/°	90	90	90
Volume/Å^3	1010.37(7)	3809.5(1)	1617.6(1)
Z	2	4	4
ρ_{calc}g/cm^3	2.307	2.225	2.364
μ/mm^{-1}	28.236	29.803	7.179
F(000)	672.0	2420.0	1080.0
Crystal size/mm	0.0577×0.0335× 0.0228	0.1167×0.0371×0.0201	0.274×0.108×0.035
Radiation	Cu Kα (λ = 1.54018)	CuKα (λ = 1.54184)	MoKα (λ = 0.71073)
2Θ range for data collection/°	8.888 to 134.314	7.124 to 124.882	6.772 to 49.412
Index ranges	$-7 \le h \le 8$, $-15 \le k \le 15$, $-11 \le l \le 11$	$-13 \le h \le 14$, $-13 \le k \le 18$, $-19 \le l \le 20$	$-10 \le h \le 10$, $-15 \le k \le 15$, $-15 \le l \le 15$
Reflections collected	8924	20551	12121
Independent reflections	3344	5862	2757
R_{int} / R_{sigma}	0.0435 / 0.0439	0.0467 / 0.0424	0.0647 / 0.0562
Data/restraints/parameters	3344/15/255	5862/40/443	2757/15/170
Goodness-of-fit on F^2	1.080	1.030	1.042
Final R indexes [I>=2σ (I)]	R_1=0.0370, wR_2=0.0874	R_1=0.0321, wR_2=0.0795	R_1=0.0391, wR_2=0.0746
Final R indexes [all data]	R_1=0.0441, wR_2=0.0924	R_1=0.0363, wR_2=0.0822	R_1=0.0521, wR_2=0.0807
Largest diff. peak/hole / eÅ^{-3}	0.94/-0.64	1.32/-0.57	1.24/-1.20
Flack parameter	-0.032(6)	-0.024(3)	-0.029(10)

Table S2. Relevant bond distances for compounds **1**, **2** and **3** from X-ray structure determination and from *in vacuo* calculations at B3LYP/6-31G(d) level of theory (in brackets).

	Compound (**1**)		Compound (**2**)		Compound (**3**)	
	Sr(1)-O(2)	2.653(9)	Sr(1)-O(2)	2.701(7)	Sr(1)-O(4)	2.580(7)
	Sr(1)-O(3)	2.615(9)	Sr(1)-O(3)	2.566(8)	Sr(1)-O(5)	2.653(7)
	Sr(1)-O(4)^{i}	2.642(9)	Sr(1)-O(10)	2.597(7)	Sr(1)-O(6)	2.704(8)
	Sr(1)-O(5)^{i}	2.754(8)	Sr(1)-O(11)	2.722(7)	Sr(1)-O(2)^{v}	2.576(7)
	Sr(1)-O(6)^{i}	2.650(9)	Sr(1)-O(12)	2.656(8)	Sr(1)-O(3)^{v}	2.640(7)
	Sr(1)-O(8)	2.685(9)	Sr(1)-O(14)^{iii}	2.714(7)	Sr(1)-O(1w)	2.623(9)
	Sr(1)-O(9)	2.563(9)	Sr(1)-O(15)^{iii}	2.605(7)	Sr(1)-O(2w)	2.578(10)
	Sr(1)-O(10)^{ii}	2.703(9)	Sr(1)-O(1w)	2.533(8)	Sr(1)-O(3w)	2.541(18)
	Sr(1)-O(11)^{ii}	2.690(9)	Sr(1)-O(2w)	2.632(8)		
			Sr(2)-O(8)	2.710(7)		
			Sr(2)-O(9)	2.558(7)		
			Sr(2)-O(16)	2.529(7)		
			Sr(2)-O(17)	2.743(7)		
			Sr(2)-O(18)	2.743(8)		
			Sr(2)-O(4)^{iv}	2.634(7)		
			Sr(2)-O(5)^{iv}	2.708(7)		
			Sr(2)-O(6)^{iv}	2.672(8)		
			Sr(2)-O(3w)	2.530(9)		
Sr···Sr	7.859 7.605		7.542 7.337 7.539		7.490 7.577	
Sr···I	4.793 5.536		5.107 5.199 5.466 5.629 5.521 5.086 5.238 5.605 5.237		3.724 5.311 5.772 5.448 5.718	
Sr···Sr av.	7.732 (8.611)		7.472 (8.292)		7.534 (7.697)	
Sr-Oav.	2.662 (2.709)		2.642 (2.745)		2.612 (2.721)	
Sr···I	5.164 (5.718)		5.343 (4.892)		5.195 (4.270)	

[i]1+X,+Y,+Z; [ii]-2-X,-1/2+Y,-1-Z; [iii]2-X,-1/2+Y,1/2-Z; [iv]1-X,1/2+Y,1/2-Z; [v]1-X,1/2+Y,3/2-Z

Table S3. List of hydrogen bonds for compounds **1**-**3**, with D-H···A < r(A) + 2.000 Å and DHA > 110°, where D= H-donor and A= H-acceptor.

Compound (1)				**Compound (2)**				**Compound (3)**			
D-H···A	D···A (Å)	H···A (Å)	DHA (°)	D-H···A	D···A (Å)	H···A (Å)	DHA (°)	D-H···A	D···A (Å)	H···A (Å)	DHA (°)
O2-H2···I1^{i}	3.841	3.230	130.59	O2-H2···I1^{i}	3.441	2.699	151.28	O2-H2···I1^{i}	3.494	2.774	146.86
O3-H3···I2	3.454	2.615	169.60	O3-H3···I1	3.394	2.576	176.16	O3-H3···I2^{ii}	3.564	2.847	147.07
O4-H4···O6	2.880	2.154	147.66	O5-H5···I3^{ii}	3.484	2.826	138.62	O4-H4···I1^{iii}	3.549	2.782	156.37
O4-H4···O9^{ii}	3.308	2.648	138.70	O6-H6···I3^{i}	3.604	2.841	155.70	O5-H5···I2^{iv}	3.537	2.926	133.13
O5-H5···I1^{iii}	3.569	2.909	139.10	O8-H8··· I1^{iii}	3.675	2.868	168.44	O6-H6···I1^{v}	3.602	2.945	138.67
O6-H6···I1^{iv}	3.505	2.808	143.97	O9-H9···I1^{i}	3.532	2.721	169.94	O1W-H1WA···I2	3.668	3.033	133.24
O8-H8···I1^{v}	3.790	3.053	145.42	O10-H10···I2^{iv}	3.745	3.154	131.26	O1W-H1WB···I2^{ii}	3.627	2.821	159.08
O9-H9···I2^{vi}	3.446	2.727	142.99	O11-H11···I2^{v}	3.525	2.749	158.59	O2W-H2WA···^{I2iv}	3.878	3.251	132.71
O10-H10···I1^{i}	3.844	3.083	155.59	O12-H12···I4^{vi}	3.610	2.878	149.73	O2W-H2WB···I1^{vi}	3.563	2.719	171.82
O11-H11···O5^{vii}	2.863	2.080	159.57	O14-H14···O4W^{vii}	2.766	1.967	164.89	C2-H2A···I1^{vii}	3.851	3.104	134.15
C1-H1A···I2^{i}	3.959	3.306	126.36	O15-H15···I3	3.400	2.622	158.74	C4-H4A···O1W^{vii}	3.482	2.541	161.04
C2-H2A···O11^{viii}	3.381	2.653	131.34	O16-H16···I2	3.462	2.669	163.19	O3W-H3WB ··O1^{viii}	2.760	2.260	115.71
C6-H6A···I2^{iii}	3.918	3.251	127.58	O17-H17···I2^{iv}	3.520	2.817	145.05	O3X-H3XA···O1^{viii}	2.778	2.099	133.40
C6-H6B···O12A^{i}	3.230	2.644	119.15	O18-H18···I1^{i}	3.791	3.050	151.53	O3X-H3XB···I1^{viii}	4.056	3.192	168.18
C7-H7A···I1^{v}	4.023	3.154	149.90	O1W-H1WB···O7^{vi}	2.933	2.335	127.64				
C8-H8A···O12B^{ix}	3.508	2.590	156.10	O2W-H2WA···I4^{viii}	3.595	2.925	137.16				
C12B-H12A···I2^{vii}	4.068	3.274	140.39	O3W-H3WA···O4W	2.699	1.922	151.24				
O12A-H12D···O11	2.871	2.446	113.36	O3W-H3WB···I3	3.775	3.159	131.24				
O12A-H12D···I1	4.077	3.264	172.09	C1-H1B···I3^{ii}	3.938	3.292	125.70				
C12A-H12E···I2^{vii}	3.982	3.058	159.78	C6-H6A···O13^{viii}	3.384	2.466	157.71				
				C7-H7A···I1^{iii}	4.011	3.178	145.03				
				C9-H9A···I4^{viii}	4.028	3.238	138.87				

				C10-H10A···I2^{iv}	3.910	3.216	129.22				
				C12-H12A···I2^{iv}	4.105	3.329	138.41				
				C18-H18B···I3^{iv}	3.922	3.202	132.36				
				O4W-H4WA···I4	3.572	2.737	167.41				
				O4W-H4WB···O1^{ix}	3.047	2.340	140.85				
i: x, y, z+1; ii: x+1, y, z; iii: -x-1, y-1/2, -z-1; iv: x+1, y, z+1; v: -x-2, y-1/2, -z-2; vi: -x-2, y+1/2, -z-1; vii: -x-1, y+1/2, -z-1; viii: -x-2, y-1/2, -z-1; ix: x-1, y, z;				i: -x+1, y+1/2, -z+1/2 ii: -x+3/2, -y+1, z-1/2 iii: x+1/2, -y+1/2, -z+1 iv: -x+2, y-1/2, -z+1/2 v: -x+3/2, -y+1, z+1/2 vi: x-1/2, -y+1/2, -z+1 vii: -x+5/2, -y+1, z-1/2 viii: x-1, y, z ix: -x+3/2, -y+1, z+1/2				i: -x+1/2, -y, z+1/2 ii: x+1/2, -y+1/2, -z+2 iii: x+1/2, -y+1/2, -z+1 iv: x-1/2, -y+1/2, -z+2 v: x-1/2, -y+1/2, -z+1 vi: -x+1/2, -y+1, z+1/2 vii: -x+1, y-1/2, -z+3/2 viii: -x, y+1/2, -z+3/2			

Section S2. Details of theoretical calculations.

The linear combination of gaussian-type function (LCGTF) approach as implemented in the CRYSTAL14 program was used throughout, in conjunction with "PS" and "AE" Hamiltonians and basis sets detailed in the main text. All the calculations were based on the experimental structures retrieved from single-crystal X-ray diffraction experiments. First, atomic coordinates were fully relaxed at fixed lattice parameters. At this stage, default thresholds[1] were selected to control the level of numerical approximation in evaluating the Coulomb and exchange series. Thresholds on total energy changes were set to 10^{-6} and 10^{-7} between subsequent cycles in the SCF and geometry optimization procedures. A 70% mixing of the Fock matrices and an eigenvalue level shift of 0.7 hartree were applied to accelerate convergence.**Error! Bookmark not defined.** The reciprocal space was sampled according to a regular sublattice defined by 4 points on each axis in the irreducible Brillouin zone (BZ). For DFT calculations, the exchange-correlation contribution to the total energy was computed using the default pruned grid**Error! Bookmark not defined.** for numerical integration, resulting in an average deviation for the electronic charge in the unit cell as low as $5(3)\cdot10^{-4}$ *e* for compound **1** and $4(2)\cdot10^{-4}$ *e* for compound **3**.

[1] Dovesi, R.; Saunders, V. R.; Roetti, C.; Orlando, R.; Zicovich-Wilson, C. M.; Pascale, F.; Civalleri, B.; Doll, K.; Harrison, N. M.; Bush, I. J.; D'Arco, P.; Llunell, M.; Causà, M.; Noël, Y. CRYSTAL14 User's Manual. University of Torino: Torino, **2014**

As the compounds here investigated bear some kind of disorder (see *infra*), the possible alternative site occupancies were taken into account as well. For each compound, geometry optimizations were repeated for all the experimentally detected independent conformations or occupations in the unit cell (see *infra*). A supercell approach, where the disorder is directly included in the model to reproduce the experimental site occupation factors, was deemed not suitable due to the impractical computational cost it would have implied.[2]

Once convergence was achieved, the coupled-perturbed (CP) Hartree-Fock/Kohn-Sham method[3–5] as implemented in the CPHF/CPKS modules of CRYSTAL14[1] was exploited to extract from the Bloch-consistent periodic wavefunction information on optical axes, dielectric tensors and first- and second-order polarizabilities. To this end, thresholds on Coulomb and exchange series were lowered to either 10^{-14} or 10^{-28}, while that on total energy change across the SCF cycles was set to 10^{-9}. A finer grid in the Pack-Monkhorst net (keyword:[1] SHRINK/10 10) was also selected. For the Hartree-Fock calculations, eigenvalue level shifter and mixing of Fock matrices were increased to 0.8 hartree and 80 %, respectively, while for the DFT PBE0 ones a Broyden scheme[6] modified according to Johnson,[7] with $W_0 = 10^{-4}$ and a 50 % mixing of the matrix second derivatives, was applied (keyword:[1] BROYDEN/0.0001 50 2).

Explorative checks showed that the CP-evaluated properties were reasonably converged with this set of parameters. Indeed, a considerably faster convergence against the BZ sampling and the number of terms in Coulomb and exchange series should be expected in large band gap systems than in the small band gap ones.[8,9] As concerns the present case, the band gap is close to 7 eV, being for example as large as 6.81 and 6.97 eV in compounds (**1**) and (**3**) respectively at the PBE0/PS theory level.

[2] For example, we found that the CPU time tCPU for the PBE0/3-21G calculations is directly proportional to the number of atoms in the asymmetric units, n_A, according to an empirical law tCPU (days) = 2.01(9) n_A - 70(5). This means that even a 2x2x1 supercell approach applied to (**1**), taking into account also the internal symmetry reduction, would roughly increase the computational time from 29 to 508 days of CPU time to achieve full convergence.

[3] Ferrero, M.; Rerat, M.; Orlando, R.; Dovesi, R. *J. Comput. Chem*. **2008**, 29, 1450-1459.
[4] Ferrero, M.; Rerat, M.; Orlando, R.; Dovesi, R. *J. Chem. Phys*. **2008**, 128, 014110.
[5] Ferrero, M. Rerat, M.; Kirtman, B.; Dovesi, R. J. *Chem. Phys*. **2008**, 129, 244110.
[6] Broyden, C. G. *Math. Comput*. **1965**, 19, 577-593.
[7] Johnson, D. D. *Phys. Rev* B, **1988**, 38, 12807-12813.
[8] Lacivita, V.; Rérat, M.; Orlando, R.; Dovesi, R.; D'Arco, P. *Theor. Chem. A*cc. **2016**, 135, 81.
[9] Lacivita, V.; Rérat, M.; Orlando, R.; Ferrero, M.; Dovesi, R. *J. Chem. Phys*. **2012**, 136, 114101.

Table S4. Effect of Hamiltonian and basis set on the predicted symmetry-independent optical tensor properties of compound **1** ($P2_1$), compound **3** ($P2_12_12_1$) and sucrose ($P2_1$). See the Experimental in the main text for the meaning of the PS and AE labels. For partly disordered crystals, values refer to perfect crystal models derived from the disorder sites with largest occupancies.

	Compound **1**				Compound **3**				Sucrose			
Method	PBE0/PS	PBE0/AE	HF/PS	HF/AE	PBE0/PS	PBE0/AE	HF/PS	HF/AE	PBE0/PS	PBE0/AE	HF/PS	HF/AE
$\chi^{(1)}_{xx}$ [a]	1.2083	0.9778	0.9594	0.7876	1.1639	0.9632	0.9752	0.7469	1.1622	1.1009	0.9993	0.8924
$\chi^{(1)}_{xz}$ [a]	-0.0067	-0.0290	-0.0112	-0.0061	0.0	0.0	0.0	0.0	-0.0435	-0.0647	-0.0307	-0.0378
$\chi^{(1)}_{yy}$ [a]	1.2714	1.1008	1.0161	0.8725	1.0521	0.8676	0.8866	0.6689	1.2136	1.1690	1.0598	0.9750
$\chi^{(1)}_{zz}$ [a]	1.2339	1.0878	0.9984	0.8585	1.0021	0.7686	0.8501	0.6168	1.1750	1.1131	1.0227	0.9186
ε_{11} [b]	2.2066	1.9707	1.9564	1.7871	2.1639	1.9632	1.9752	1.7469	2.1247	2.0420	1.9782	1.8654
ε_{22} [b]	2.2714	2.1008	2.0161	1.8725	2.0521	1.8676	1.8866	1.6689	2.2136	2.1690	2.0598	1.9750
ε_{33} [b]	2.2355	2.0950	2.0013	1.8590	2.0021	1.7686	1.8501	1.6168	2.2125	2.1719	2.0438	1.9455
$\chi^{(2)}_{xxy}$ [c]	1.0643	0.5247	0.5271	0.4501	0.0	0.0	0.0	0.0	0.1447	-0.0246	0.1171	0.1362
$\chi^{(2)}_{xyz}$ [c]	-0.2388	-0.3892	-0.1559	-0.1864	-0.1406	-0.1025	-0.1023	-0.0547	-0.0013	-0.0381	-0.0032	0.0085
$\chi^{(2)}_{yyy}$ [c]	-0.7354	-0.7009	-0.4130	-0.4953	0.0	0.0	0.0	0.0	0.2885	0.2289	0.2582	0.2900
$\chi^{(2)}_{yzz}$ [c]	-0.4415	-0.1541	-0.2396	-0.2067	0.0	0.0	0.0	0.0	0.2048	0.0998	0.1384	0.1313

[a] First-order electric susceptivity tensor (dimensionless).

[b] Diagonalized dielectric tensor (dimensionless).

[c] Second-order electric susceptivity, in atomic units. The same quantities can be expressed in other conventions through the usual conversion factors. Frequent alternative expressions of the second order tensor components as β_{ijk} or d_{ijk} quantities (always in atomic units) are $\beta_{ijk} = (V \cdot \chi_{ijk}) / 2\pi$, V being the unit cell volume in cubic bohr, and $d_{ijk} = \chi_{ijk} / 2$. Conversion to the MKS system in terms of reciprocal electric field units can be accomplished according to d_{ijk}(MKS) = d_{ijk}(a.u.)/0.514220632 pm/V. See also www.physics.nist.gov/constants.

Table S5. As Table S4 above, referring to perfect crystal models derived from the disorder sites with lowest occupancies.

	Compound **1**				Compound **3**			
Method	PBE0/PS	PBE0/AE	HF/PS	HF/AE	PBE0/PS	PBE0/AE	HF/PS	HF/AE
$\chi^{(1)}_{xx}$ [a]	1.2183	1.0089	0.9616	0.7966	1.1386	0.9611	0.8857	0.7260
$\chi^{(1)}_{xz}$ [a]	-0.0211	-0.0535	-0.0206	-0.0234	0.0	0.0	0	0.0
$\chi^{(1)}_{yy}$ [a]	1.2757	1.1088	1.0155	0.8670	1.0711	0.8421	0.8539	0.6692
$\chi^{(1)}_{zz}$ [a]	1.2171	1.0428	0.9863	0.8420	0.9958	0.7874	0.8044	0.6339
ε_{11} [b]	2.2388	1.9698	1.9499	1.7867	2.1386	1.9611	1.8857	1.7260
ε_{22} [b]	2.2757	2.1088	2.0155	1.8670	2.0711	1.8421	1.8539	1.6692
ε_{33} [b]	2.1966	2.0820	1.9980	1.8519	1.9958	1.7874	1.8044	1.6339
$\chi^{(2)}_{xxy}$ [c]	1.2055	0.7148	0.6192	0.5458	0.0	0.0	0.0	0.0
$\chi^{(2)}_{xyz}$ [c]	-0.1708	-0.3192	-0.0756	-0.1030	-0.1801	-0.2131	-0.0898	-0.0961
$\chi^{(2)}_{yyy}$ [c]	0.5362	0.5360	0.3308	0.3232	0.0	0.0	0.0	0.0
$\chi^{(2)}_{yzz}$ [c]	-0.5404	-0.3303	-0.1794	-0.1842	0.0	0.0	0.0	0.0

[a] First-order electric susceptivity tensor (dimensionless).
[b] Diagonalized dielectric tensor (dimensionless).
[c] Second-order electric susceptivity, in atomic units. The same quantities can be expressed in other conventions through the usual conversion factors. Frequent alternative expressions of the second order tensor components as β_{ijk} or d_{ijk} quantities (always in atomic units) are $\beta_{ijk} = (V \cdot \chi_{ijk}) / 2\pi$, V being the unit cell volume in cubic bohr, and $d_{ijk} = \chi_{ijk} / 2$. Conversion to the MKS system in terms of reciprocal electric field units can be accomplished according to d_{ijk}(MKS) = d_{ijk}(a.u.)/0.514220632 pm/V. See also www.physics.nist.gov/constants.

Table S6. Short intermolecular hydrogen bonded contacts O-H···X, X = O, I^- involving disordered groups in compounds **1** and **3**, as optimized at the PBE0/PS theory level (see Experimental section in the paper).

Substance	Site [a]	sof / % [b]	Contact	$d_{H\cdots X}$ / Å	$d_{O\cdots X}$ / Å	α_{OHX} / deg	Symmetry [c]
(**1**)	A	58.9	O-H···I^-	2.67	3.483	141.1	x, –1+y, z
	B	41.1	O-H···O	1.94	2.870	160.6	x, –1+y, z
(**3**)	A	56.7	O-H···I^- O-H···O	2.74 1.87	3.442 2.784	130.1 156.6	x, y, –1+z –x,1/2+y,–1/2–z
	B	43.3	O-H···I^- O-H···O	3.05 1.86	3.895 2.794	146.5 159.8	–1/2+x,1/2–y,–z –x,1/2+y,–1/2–z

[a] For compound **1**, "A" and "B" sites imply a different orientation of a terminal $–CH_2OH$ chain, whereas for compound **3** they mark the different position of a co-crystallized water molecule (see text).
[b] Site occupation factor (dimensionless, percent units).
[c] Symmetry operation which generates the acceptor group X.

Table S7. Symmetry-allowed second electric susceptibility tensor elements, d_{ijk}, for compound **1** (MKS units, $pm \cdot V^{-1}$), as a function of the different level of theory adopted in LCGTF periodic calculations. Label PS means 6-31G* basis set, including Hay-Wadt pseudopotentials on Sr and I ions, while the AE one refers to an all-electron 3-21G basis set (see the main text). "A" and "B" refer to different disorder site occupations, with site occupation factors as large as 58.9 % and 41.1 % (see the main text).

	Compound **1**							
	PBE0/PS		PBE0/AE		HF/PS		HF/AE	
	A	B	A	B	A	B	A	B
d_{xxy}	1.03487	1.17216	0.51019	0.69503	0.51252	0.60208	0.43765	0.53071
d_{xyz}	-0.23220	-0.16608	-0.37844	-0.31037	-0.15159	-0.07351	-0.18125	-0.10015
d_{yyy}	-0.71506	0.52137	-0.68152	0.52118	-0.40158	0.32165	-0.48160	0.31426
d_{zzy}	-0.42929	-0.52546	-0.14984	-0.32117	-0.23297	-0.17444	-0.20098	-0.17911
	Compound **3**							
d_{xyz}	-0.13671	-0.17512	-0.09967	-0.20721	-0.09947	-0.08732	-0.05319	-0.09344
Sucrose (not disordered)								
d_{xxy}	0.14070		-0.02392		0.11386		0.13243	
d_{xyz}	-0.00126		-0.03705		-0.00311		0.00826	
d_{yyy}	0.28052		0.22257		0.25106		0.28198	
d_{zzy}	0.19914		0.09704		0.13457		0.12767	

Table S8. Ratio between the average second-order squared susceptibility tensor elements of compounds **1** and **3** with respect to crystalline sucrose, as a function of the level of theory adopted in LCGTF periodic calculations. Label PS means 6-31G* basis set, including Hay-Wadt pseudopotentials on Sr and I ions, while the AE one refers to an all-electron 3-21G basis set (see the main text).

	$<d_{ijk}^2>/<d_{ijk}^2>_{sucrose}$			
	PBE0/PS	PBE0/AE	HF/PS	HF/AE
Compound **1**	17.61	22.21	7.25	5.21
Compound **3**	1.18	3.07	0.74	0.35

Table S9. Symmetry-independent second-order susceptivity tensor elements (atomic units) for organic and inorganic substructures in compounds **1** and **3**, as a function of the computational level. The most populated disordered site was always considered.

	PBE0/PS		PBE0/AE		HF/PS		HF/AE	
compound **1**								
	Fructose	Ions	Fructose	Ions	Fructose	Ions	Fructose	Ions
$\chi^{(2)}_{xxy}$	0.0260	-0.3376	0.1291	-0.0004	0.0055	-0.0167	0.0174	-0.0001
$\chi^{(2)}_{xyz}$	0.0009	-0.2467	-0.0151	0.0005	-0.0006	-0.0155	0.0016	0.0003
$\chi^{(2)}_{yyy}$	0.1652	2.0123	0.3413	0.0042	0.0947	0.0422	0.1056	0.0027
$\chi^{(2)}_{yzz}$	-0.3139	-1.2015	-0.2963	-0.0001	-0.1185	-0.0278	-0.1431	0.0001

compound **3**												
	Fructose	Ions	Water	Fructose	Ions	Water	Fructose	Ions	Water	Fructose	Ions	Water
$\chi^{(2)}_{xyz}$	0.0158	0.1031	0.0094	0.0294	0.0003	0.0137	-0.0135	0.0086	0.0086	0.0093	0.0003	0.0046

As detailed in the main text, the ions invariably provide the largest absolute tensor elements at the PBE0/PS theory level, while at lower theory levels the opposite is true, with the sugar bearing the highest contributions. Moreover, when the 3-21G all-electron basis set is considered, $\chi_{ijk}^{(2)}$'s from ions almost completely vanish. This likely indicates that the AE basis set somehow misses the contributions of polarizable electrons in the valence region of heavy atoms. This contribution can be at least partly retrieved employing suitable pseudopotentials (compare for example the HF/PS column in Table 6 with the HF/AE one), but if correlation effects are not taken into account as well, the nonlinear contribution from the inorganic substructure turns out to be significantly underestimated (compare the PBE0/PS column in Tables 9s and 10s with the HF/PS one).

Remarkably, this explains the behaviour of the estimated square averaged tensor elements $\langle d_{ijk}^2 \rangle$ as a function of the computational method (Figure 7), as in both compounds **1** and **3** they increase on going from HF/AE to PBE0/PS. In sucrose, where no heavy atoms are present, changes in estimated $\langle d_{ijk}^2 \rangle$ are much smaller and non-monotonic.

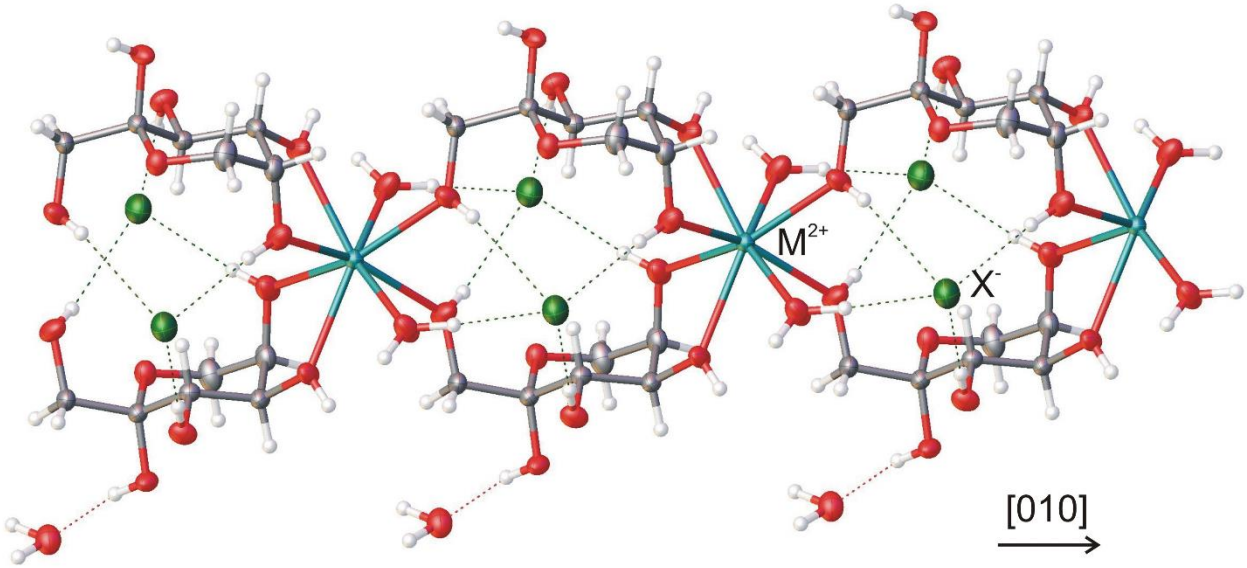

Figure S1. Isomorphic fragment $[M(fructose)_2(H_2O)_2]X_2{\cdot}H_2O$ of the *in vacuo* explorative calculations pertaining to compounds with Cl^- and Br^-, where the anion X was substituted with iodine.

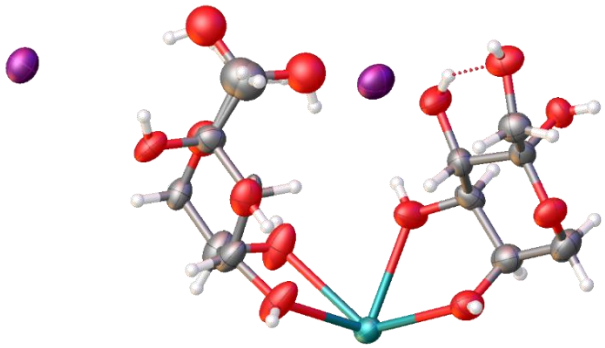

Figure S2. Asymmetric unit of compound **1**, with thermal ellipsoids for all atoms except hydrogens.

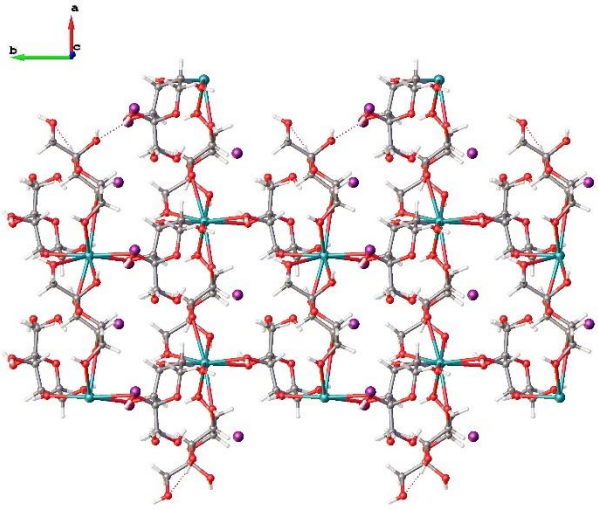

Figure S3. View of compound **1** in the (001) plane.

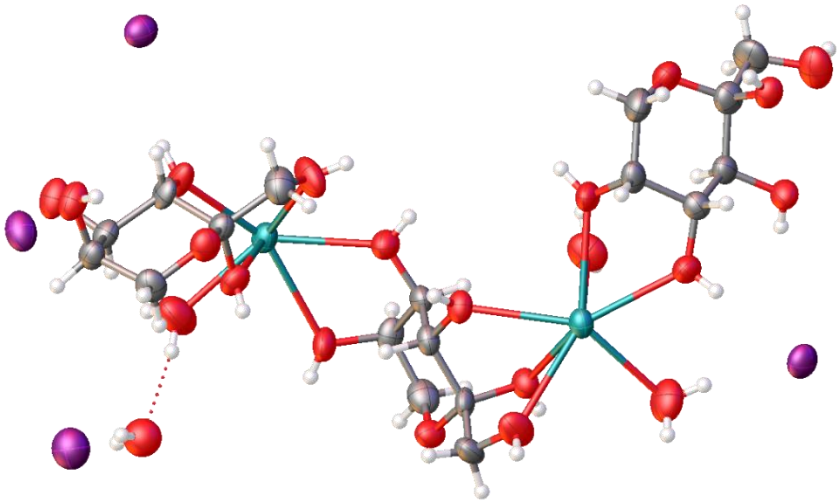

Figure S4. Asymmetric unit of compound **2**, with thermal ellipsoids for all atoms except hydrogens.

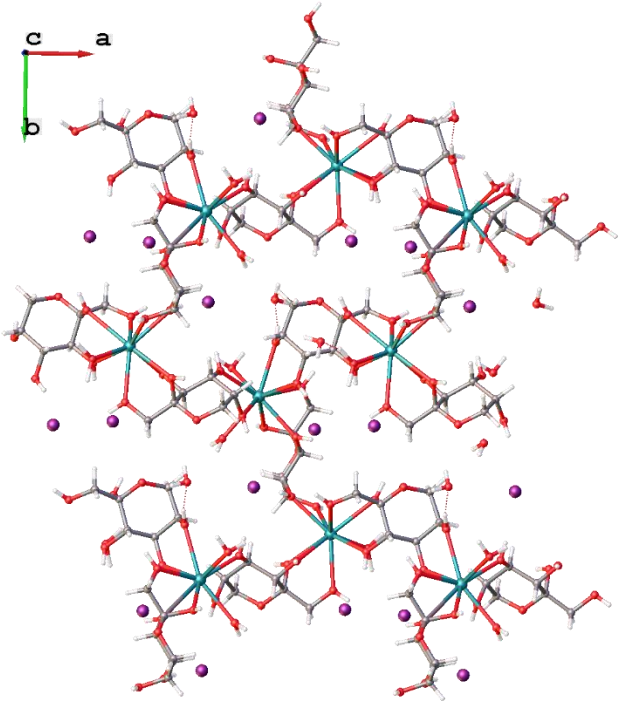

Figure S5. View of compound **2** in the (001) plane.

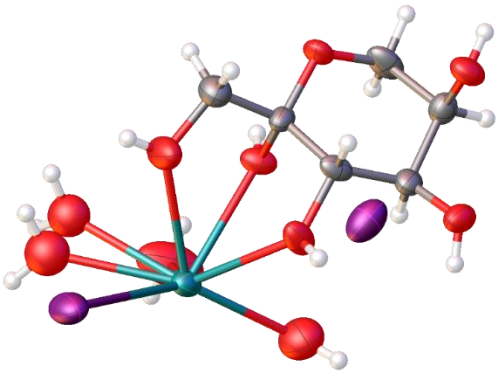

Figure S6. Asymmetric unit of compound **3**, with thermal ellipsoids for all atoms except hydrogens.

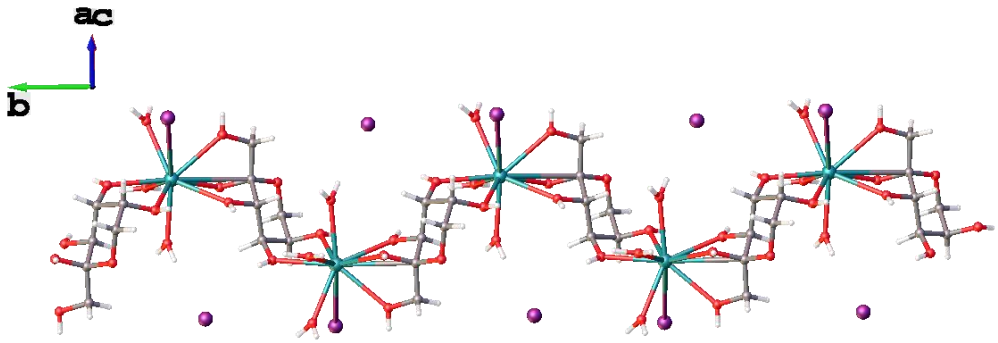

Figure S7. View of compound **3** along the *b* axis.

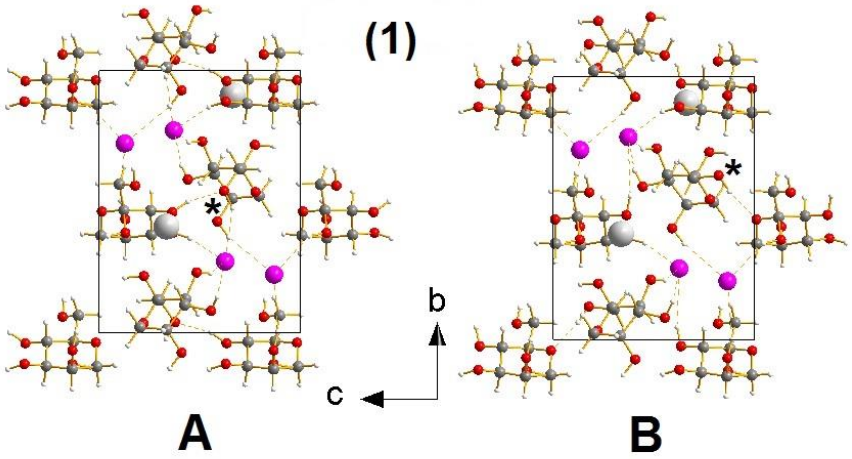

Figure S8. Crystal packing along the *a* axis of the perfectly ordered structures of compound (**1**), starting from the two allowed A and B conformers in the disordered experimental structure, as derived from PBE0/PS geometry optimizations in the solid state. See the main text for more details. Short H···X hydrogen bonded contacts (1.8 Å $\leq d_{H\cdots X} \leq$ 3.1 Å) are shown as red dashed lines. A star "*" marks the two different orientations of the $-CH_2OH$ chain in one fructose molecule.

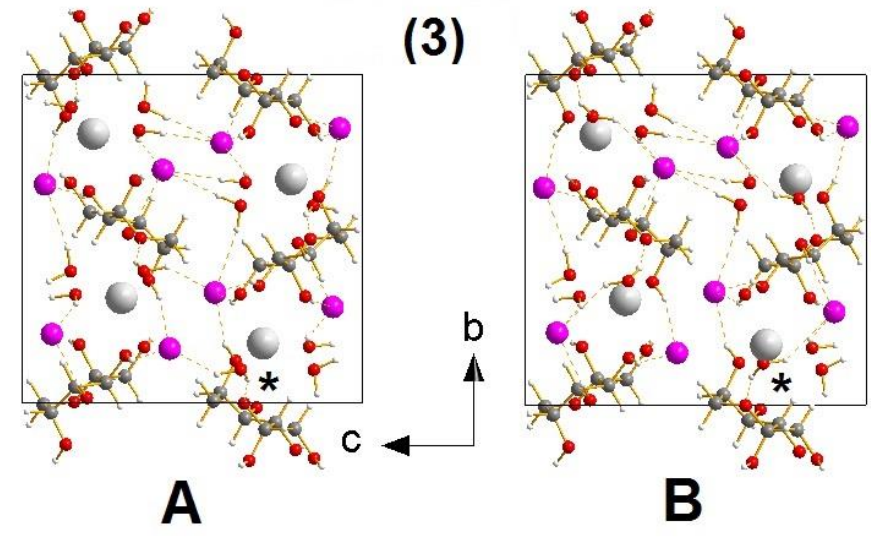

Figure S9. As Figure S1 above, for the structures derived from compound (**3**). A star "*" marks here the two different position of the disordered O3w water molecule.

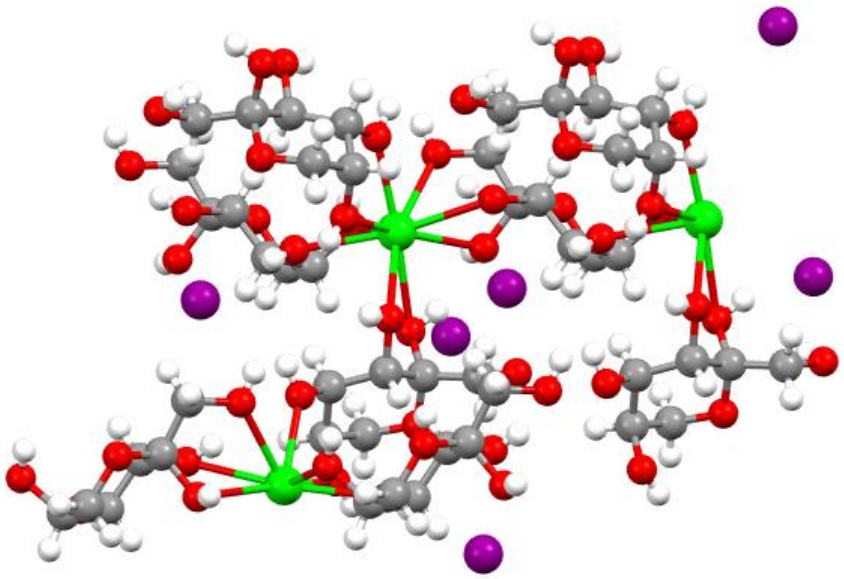

Figure S10. Fragment analyzed in the *in vacuo* calculations of compound (**1**).

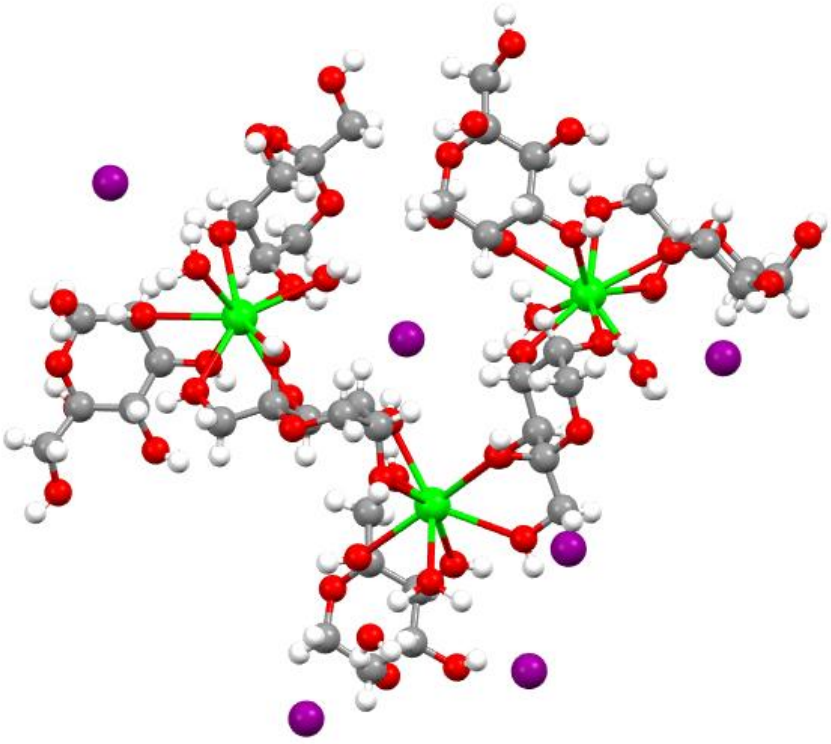

Figure S11. Fragment analyzed in the *in vacuo* calculations of compound (**2**).

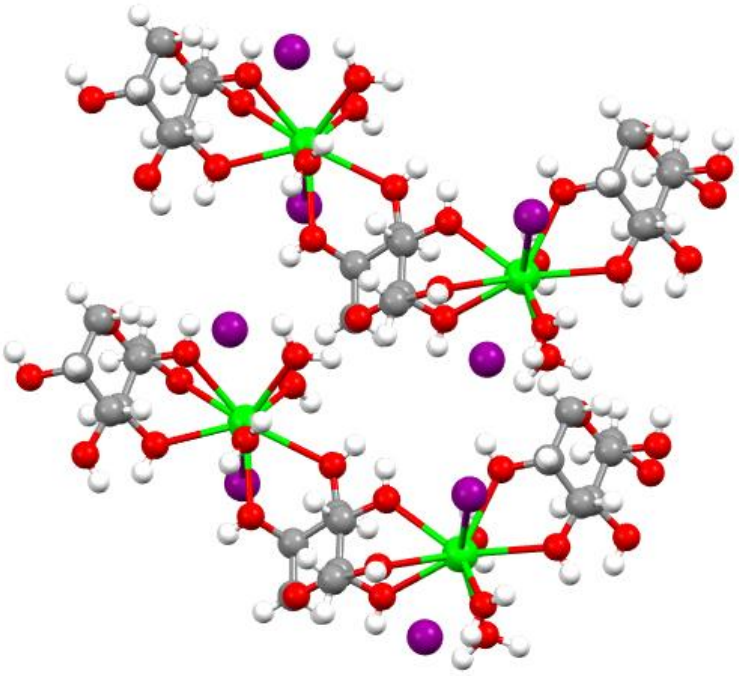

Figure S12. Fragment analyzed in the *in vacuo* calculations of compound (**3**).

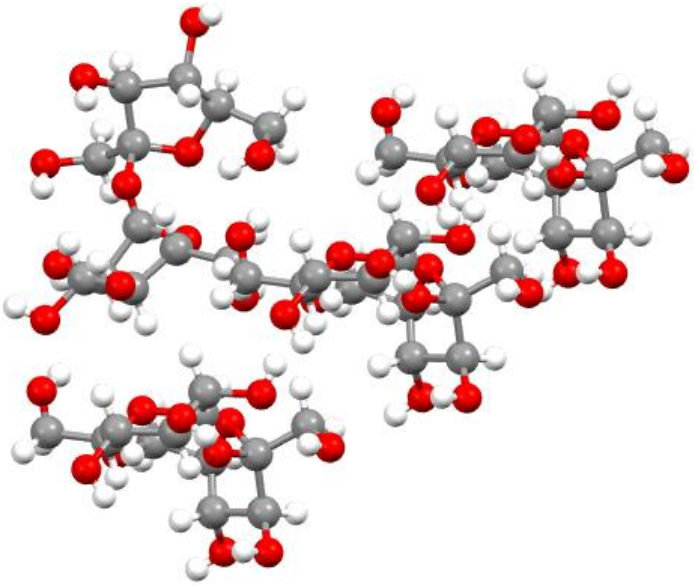

Figure S13. Fragment analyzed in the *in vacuo* calculations of sucrose.